An assessment of climate feedback processes using satellite observations of clear-sky OLR

Eui-Seok Chung,[1] David Yeomans,[1] and Brian J. Soden[1]

Received 23 November 2009; accepted 7 December 2009; published 20 January 2010.

[1] Clear-sky longwave radiative feedback processes depicted in climate models prepared for the Intergovernmental Panel on Climate Change (IPCC) Fourth Assessment Report (AR4) are investigated using satellite observations of the clear-sky outgoing longwave radiation (OLR). Estimates of clear-sky longwave radiative damping are derived from regional, seasonal, and interannual sources of variability. In spite of well-known biases of tropospheric temperature and humidity in climate models, comparisons indicate that the intermodel range in the rate of clear-sky radiative damping are small despite large intermodel variability in the mean clear-sky OLR. Moreover, the model-simulated rates of radiative damping are consistent with those obtained from satellite observations and are indicative of a strong positive correlation between temperature and water vapor variations over a broad range of spatiotemporal scales. **Citation:** Chung, E.-S., D. Yeomans, and B. J. Soden (2010), An assessment of climate feedback processes using satellite observations of clear-sky OLR, *Geophys. Res. Lett.*, *37*, L02702, doi:10.1029/2009GL041889.

1. Introduction

[2] Climate models have been widely used to predict future climate change due to the projected increase in anthropogenic greenhouse gases. In order to enhance the credibility of climate change projections, it is necessary to evaluate the quality of parameterization schemes employed to represent various climate feedback processes using in-situ and satellite observations, and to intercompare the performances of models used in climate assessments [*Zhang et al.*, 1994; *Potter and Cess*, 2004; *Allan*, 2009].

[3] Outgoing longwave radiation (OLR) at the top of the atmosphere (TOA) is the facets of interactions of the surface and atmosphere due to the changes in temperature, cloud, and humidity in response to the incoming solar radiation, and the anthropogenic forcings caused by the increase in greenhouse gases. It provides a useful metric to evaluate the reliability and consistency of climate feedback processes depicted in climate models [e.g., *Cess et al.*, 1990; *Slingo et al.*, 2000; *Potter and Cess*, 2004; *Soden and Held*, 2006].

[4] Although it is well known that the intermodel differences in climate sensitivity to external forcings are mainly caused by the difference in cloud feedback process [e.g., *Potter and Cess*, 2004; *Soden and Held*, 2006], discrepancies between climate models still exist for non-cloud feedback processes [e.g., *Cess et al.*, 1990; *Colman*, 2003; *Soden and Held*, 2006]. In addition, the atmospheric conditions associated with cloud formation and development are quite different from cloud free cases, implying that uncertainty in non-cloud feedback processes may hinder an assessment of the contribution of cloud feedback process to climate sensitivity [e.g., *Zhang et al.*, 1994; *Sohn and Bennartz*, 2008]. Current generation climate models also exhibit significant biases in tropospheric temperature and humidity compared to satellite observations [*John and Soden*, 2007]. Since the clear-sky OLR is highly sensitive to temperature and atmospheric water vapor (and also anthropogenic greenhouse gases and aerosols), it is useful to evaluate the sensitivity of clear-sky OLR to changes in temperature and water vapor arising from different sources of observable climate variability [e.g., *Allan*, 2006].

[5] In this study, we investigate the rate of clear-sky longwave radiative damping over a range of space and time scales to evaluate the physical processes which regulate clear-sky longwave feedbacks in climate models and assess their performance relative to satellite observations.

2. Datasets

[6] Outputs of IPCC AR4 Atmospheric Model Intercomparison Project (AMIP) are used to examine the clear-sky longwave radiative damping in climate models. This analysis focuses solely on the atmospheric-only models, in which realistic monthly mean sea surface temperature and sea ice data (from 1979 to near present) were employed to constrain simulations. A total of 11 climate model outputs (clear-sky OLR and surface temperature) are extracted from the IPCC AR4 archive: GFDL-CM2.1, CNRM-CM3, GISS ER, INMCM3, IPSL, MIROC3.2-hires, MIROC3.2-medres, MPI ECHAM5, MRI CGCM2-3.2a, NCAR CCSM3, and UKMO HADGEM1.

[7] In order to assess the clear-sky radiative damping rates depicted in these models, we employ clear-sky OLR (S-4 version) observed from the Earth Radiation Budget Experiment (ERBE) [*Barkstrom et al.*, 1989] as a reference. Monthly mean data from January 1985 to December 1988 are downloaded from the NASA Langley Atmospheric Science Data Center. In addition, clear-sky OLR observed from the Clouds and the Earth's Radiant Energy System (CERES) [*Wong et al.*, 2000] onboard both Terra and Aqua satellites are used to examine any difference compared to the results derived from EBRE measurements. ERBE-like monthly mean clear-sky OLR (ES-4 version) for 4-year period (January 2005–December 2008) is used for consistency with ERBE observations (i.e., Terra FM2-Edition1-CV and Aqua FM3-Edition1-CV).

[8] For surface temperature information, we use the European Centre for Medium-Range Weather Forecasts

[1]Rosenstiel School of Marine and Atmospheric Science, University of Miami, Miami, Florida, USA.

0094-8276/10/2009GL041889$05.00

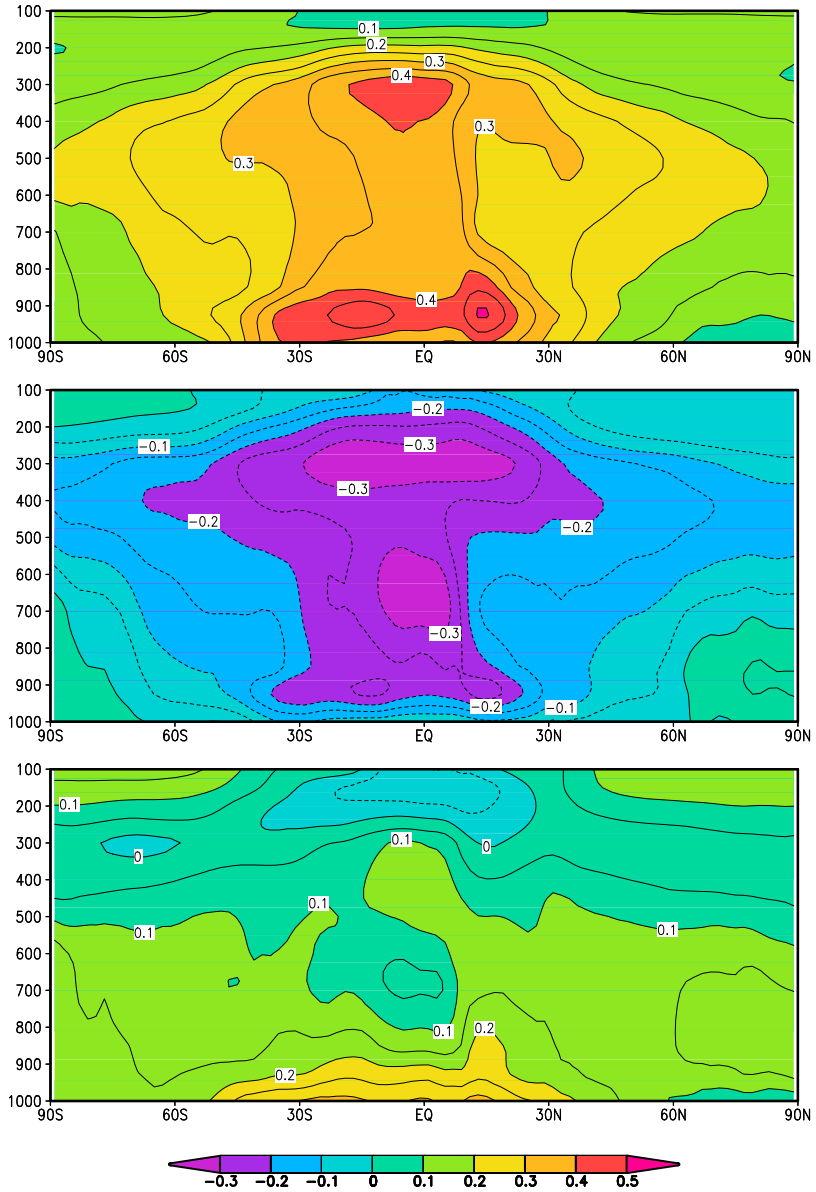

Figure 1. The zonal-mean, annual-mean distribution of radiative kernels for clear-sky conditions under the idealized assumption of a horizontally and vertically uniform temperature change of 1-K with holding relative humidity fixed: (top) temperature kernel, (middle) water vapor kernel, and (bottom) the sum of temperature and water vapor kernels. Units are W m^{-2} K^{-1}/100 mb.

(ECMWF) 40 Year Reanalysis (ERA-40) [*Uppala et al.*, 2005] for the ERBE case. However, due to the data availability, ERA-40 data is replaced by the National Centers for Environmental Prediction/National Center for Atmospheric Research (NCEP/NCAR) Reanalysis data [*Kalnay et al.*, 1996] for the period January 2005 to December 2008.

3. Results and Discussions

3.1. Idealized Radiative Damping Calculations

[9] In order to understand the sensitivity of clear-sky OLR to incremental changes in temperature and moisture, we calculated radiative kernels for the mean of all AMIP models following *Soden et al.*'s [2008] method. The kernels depend only on the radiative transfer and the unperturbed climate state and allow one to quantify the impact of temperature or moisture changes in different regions of the atmosphere on the clear-sky OLR.

[10] Figure 1 displays the zonal-mean, annual-mean kernels for temperature (Figure 1, top) and water vapor (Figure 1, middle) under clear-sky conditions. The temperature kernel describes the response of the clear-sky OLR to incremental increases in temperature of 1-K and has units of W m^{-2} K^{-1}/100 mb. If temperatures change uniformly, the kernel illustrates the contribution of different latitudes and levels to the change in OLR. The values are positive, indicating that an increase in temperature increases the clear-sky OLR. The vertically-integrated global, annual mean of temperature kernel for clear sky conditions is

approximately 3.6 W m^{-2} K^{-1}; i.e., if there are no changes in any other quantities (carbon dioxide, water vapor, clouds, etc.) and under the idealized assumption of a horizontally and vertically uniform temperature change, the global-mean clear-sky OLR should increase by 3.6 W m^{-2} for every 1-K increase in surface temperature.

[11] The water vapor kernel (Figure 1, middle) depicts the change in clear-sky OLR in response to an increase in water vapor mixing ratio that would arise from a 1-K increase in temperature while holding relative humidity (RH) fixed. The assumption of constant relative humidity is a frequent starting point in most debates on water vapor feedback and, on a global scale, is consistent with climate model predictions. Because water vapor is the strongest greenhouse gas in the atmosphere, negative values are dominant in the distribution of water vapor kernel. Therefore, increase in water vapor concentration decreases the TOA clear-sky OLR. The highest sensitivities are found over the deep tropics. In particular, the tropical free troposphere exhibits high sensitivity with approximately uniform values ranging from -0.3 to -0.2. The vertically integrated global, annual mean of water vapor kernel for clear-sky conditions is -1.6 W m^{-2} K^{-1}.

[12] The sum of temperature and water vapor kernels (Figure 1, bottom) illustrates the combined effect of the temperature and water vapor perturbations on the clear-sky OLR under the assumption of a horizontally and vertically uniform temperature change and constant relative humidity. The globally-averaged value of this combined temperature-water vapor kernel is 2.0 W m^{-2} K^{-1}. One striking feature of the fixed-RH kernel is the small values in the tropical upper troposphere, where the positive OLR response to a temperature increase is offset by negative responses to the corresponding vapor increase. Thus under a constant RH-warming scenario, the tropical upper troposphere is in a runaway greenhouse state – the stabilizing effect of atmospheric warming is neutralized by the increased absorption from water vapor. Of course, the tropical upper troposphere is not isolated but is closely tied to the lower tropical troposphere where the combined temperature-water vapor responses are safely stabilizing.

[13] Nevertheless, these small values in the tropical troposphere are important for understanding the OLR sensitivity. If one assumes that relative humidity remains fixed, then the magnitude of warming in the upper troposphere is of little consequence in modifying the clear-sky OLR. Rather, it is the trends in the relative humidity, not temperature, that are of primary importance for generating an OLR response from this region of the atmosphere. In particular, the relative humidity must decrease in order for the combined temperature and vapor changes in this region to produce a significant negative feedback on the climate system.

[14] Here we extend the studies of *Raval and Ramanathan* [1989] and *Slingo et al.* [2000] by using radiative kernels to help interpret the rate of clear-sky radiative damping obtained from both climate model simulations and satellite observations. By examining observed relationships between clear-sky OLR and surface temperature, we demonstrate a strong covariance between temperature and water vapor that is robust across all models, is quantitatively consistent with satellite observations, and when globally-averaged requires the presence of strong positive correlations between water vapor and temperature variations over a broad range of space and time scales.

3.2. Comparison of Clear-sky Radiative Damping Rates from Satellite Observations and Multi-model Ensemble Mean

[15] Figure 2 (left) shows the relations between surface temperature from ERA-40 and the corresponding clear-sky OLR obtained from the ERBE observations for the period January 1985 to December 1988 for regional (Figure 2a), seasonal (Figure 2b), and interannual variations (Figure 2c). Because of data availability and deficiencies in clear-sky classification over ice-covered surfaces, polar regions (i.e., poleward of 70°) are excluded in the analysis. The rate of radiative damping for regional variations is determined by averaging each variable for the 4-year period at each grid point and then by linearly-regressing the 4-year averaged values. As found by *Raval and Ramanathan* [1989], surface temperature and clear-sky OLR exhibit a distinct linear relation with a correlation coefficient of 0.98. A linear least-square analysis yields a slope of 2.19 W m^{-2} K^{-1} with very small uncertainty, indicating that the combination of water vapor and lapse rate changes substantially reduces the rate of clear-sky radiative damping relative to that expected from uniform temperature change of 1-K.

[16] We extend the regional analysis by considering seasonal correlations between temperature and clear-sky OLR. After constructing the 4-year mean seasonal cycle at each grid point, area-weighted global means are computed for each month and used for this analysis. Because the northern hemisphere has much larger fraction of landmass compared to its counterpart, the global mean surface temperature is the highest during the boreal summer, and vice versa. Such an annual cycle of surface temperature results in a similar annual cycle of clear-sky OLR through Stefan-Boltzmann Law (Figure 2b). The rate of radiative damping computed via linear regression yields a remarkably similar slope (2.30 ± 1.20 W m^{-2} K^{-1}) compared to that obtained from the regional regression. In both cases, the reduction of the clear-sky radiative damping rate below 3.6 W m^{-2} K^{-1} requires water vapor variations to be positively correlated with changes in temperature, such that when taken at a global-scale, the slope is similar to that expected from a constant relative humidity moistening [e.g., *Allan*, 2006, 2009].

[17] To further examine the robustness of this relation Figure 2c depicts the regression between interannual anomalies of surface temperature and clear-sky OLR. The mean seasonal cycle is removed for each grid point, and then area-weighted averaging is performed to compute global-mean interannual anomalies for the 4-year period. The primary cause of interannual variability for this period is the 1987/88 ENSO event during which higher values of surface temperature resulted in increased clear-sky OLR. The rate of radiative damping computed from linear regression over this period (2.41 ± 0.12 W m^{-2} K^{-1}) is remarkably consistent with that obtained from the regional and seasonal analyses, demonstrating a coherent relation between the radiative impact of temperature and water vapor variations over a range of space and time scales. Meanwhile, for all-sky conditions, *Lindzen and Choi* [2009] derived a

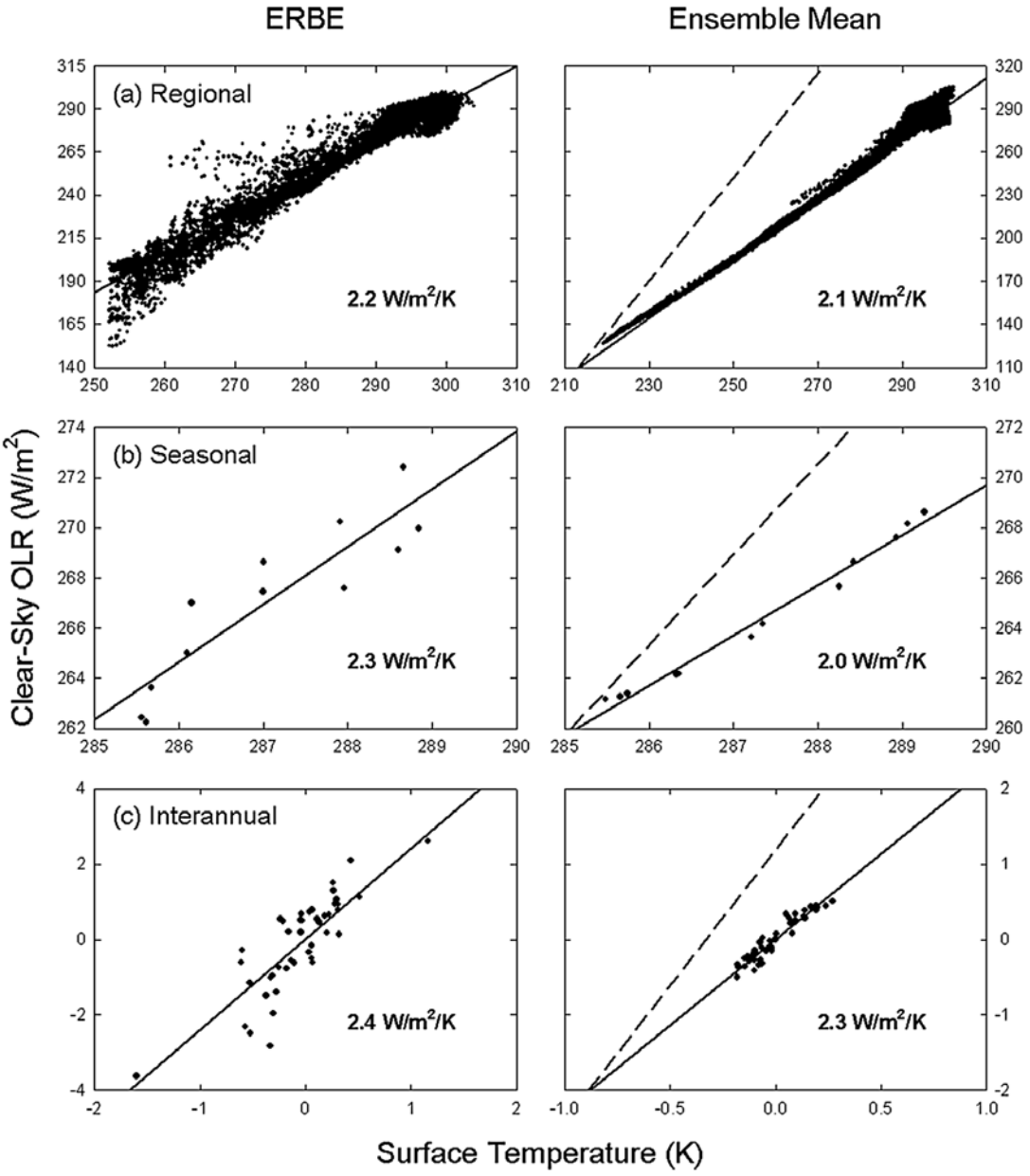

Figure 2. Scatterplots of surface temperature versus clear-sky OLR for the period 1985 to 1988: (a) regional, (b) seasonal, and (c) interannual variations. Relations are derived from (left) ERBE observations and (right) multi-model ensemble mean of 11 climate models. Ice-covered polar regions are excluded for ERBE case. Solid lines with values in W m^{-2} K^{-1} indicate the linear least-square fit, implying the clear-sky radiative damping rates. In addition, slope of dashed lines in the right panels is 3.6 W m^{-2} K^{-1}.

negative feedback process using net outgoing radiative fluxes over the tropics. However, it is difficult to directly compare our result with *Lindzen and Choi*'s [2009] due to the differences in dataset and analyzed conditions.

[18] The observed rates of radiative damping from regional, seasonal, and interannual variations are substantially smaller than the rate of Planck radiative damping (3.6 W m^{-2} K^{-1}), yet slightly larger than that anticipated from a uniform warming, constant-RH response (2.0 W m^{-2} K^{-1}). Such difference could be attributable to either variations in relative humidity and/or departures from non-uniform warming. To better evaluate the implications of such metrics, it is useful to directly compare the observed rates of radiative damping to those obtained from climate models subjected to the same analysis.

[19] Figure 2 (right) shows the relation between surface temperature and clear-sky OLR for an ensemble mean of 11 climate models. The slopes for regional, seasonal, and interannual variations are very similar to the values determined from ERBE observations, highlighting that climate models can reproduce the clear-sky longwave radiative damping in consistent with satellite observations. Considering that significantly positive response of water vapor to temperature change is essential for this radiative damping

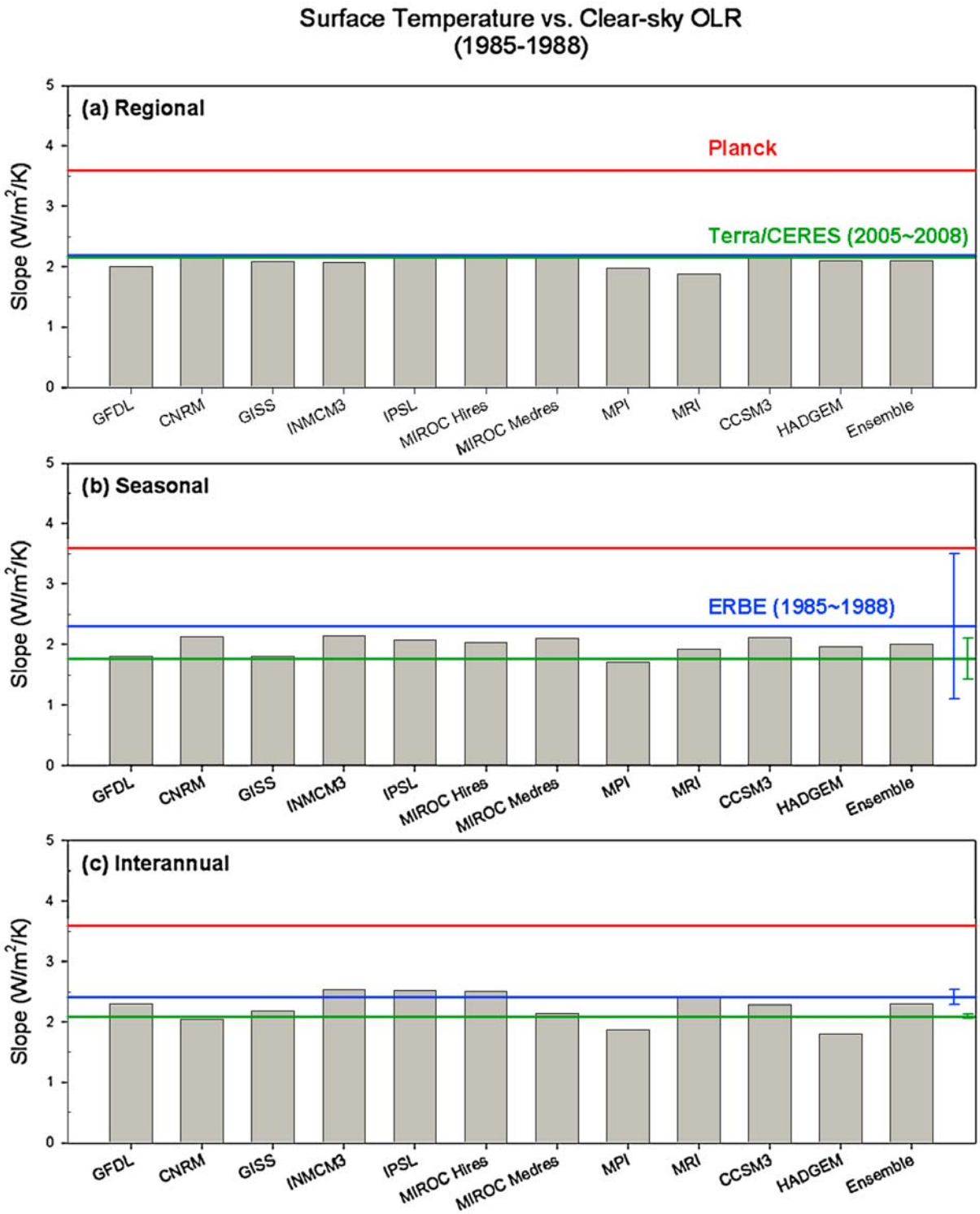

Figure 3. Intercomparisons of the slopes of clear-sky OLR to surface temperature between 11 climate models together with multi-model ensemble mean: (a) regional, (b) seasonal, and (c) interannual variations. Red lines indicate the value of Planck radiative damping rate (3.6 W m^{-2} K^{-1}). In addition, blue and green lines denote the values determined from ERBE observations for the period 1985–1988 and Terra/CERES observations for the period 2005–2008, respectively. Vertical error bars represent the slope uncertainties for ERBE and Terra/CERES.

(Figure 1, bottom), good agreement between satellite observations and model simulation confirms the robustness of positive water vapor feedback [e.g., *Soden and Held*, 2006; *Allan*, 2009].

3.3. Intercomparison of Performance between Climate Models

[20] Figure 3 intercompares the slope of clear-sky OLR to surface temperature for 11 climate models together with the

multi-model ensemble mean. Also shown are the value of Planck radiative damping rate (red line) and the slope determined from ERBE observations (blue line). Vertical error bars denote the uncertainty of the slope derived from ERBE observations. Slope uncertainties are computed by using variance of residuals, which are defined as deviation of the original data point from the regression line, together with the lag-1 autocorrelation of the residuals [e.g., *Weatherhead et al.*, 1998]. In addition, the degree of freedom is calculated as $N \times (1 - \varphi)/(1 + \varphi)$, where N and φ denote the number of data and the lag-1 autocorrelation, respectively. Although the slopes are slightly smaller than that of ERBE observations, most of climate models are consistent with each other for regional variation case (Figure 3a). The slight intermodel difference is in line with previous results that climate models denote much smaller intermodel variability for the combined feedback from water vapor and lapse rate in comparison to that for each feedback separately [e.g., *Zhang et al.*, 1994; *Soden and Held*, 2006].

[21] Compared to the regional variations, a much larger difference in slope between ERBE observations and climate models is shown for seasonal variations (Figure 3b). GFDL, GISS, and MPI exhibit distinctly smaller slopes, indicating that these models produce a noticeably positive climate feedback compared to ERBE results. However, the standard deviation of slopes between models (0.14 W m^{-2} K^{-1}) is substantially smaller than the uncertainty of slope derived from ERBE observations.

[22] A more significant intermodel variability with standard deviation of 0.29 W m^{-2} K^{-1} is illustrated in the case of interannual variations (Figure 3c). Noticeably smaller slopes shown in MPI and HADGEM compared to ERBE observations are consistent with a more strongly positive water vapor feedback and/or less negative lapse rate feedback [e.g., *Soden and Held*, 2006]. The other models are generally consistent with ERBE observations. Meanwhile, it is noted that consistent results are obtained for different time period and a longer time-scale (see Figure S1 of the auxiliary material).[1]

3.4. Radiative Damping Rates Derived from CERES Observations

[23] Clear-sky OLR observed from CERES onboard both Terra and Aqua satellites are employed to investigate whether the clear-sky longwave climate feedback parameter depends on different time period and/or different satellite observations. Green lines in Figure 3 denote the slopes derived from Terra/CERES for the period 2005 to 2008, with vertical error bars representing slope uncertainty. Due to nearly identical pattern, results from Aqua/CERES are not shown in Figure 3.

[24] While the slope and uncertainty estimated from CERES observations are almost the same as those from ERBE observations for regional variations, significant differences are noted for the cases of seasonal and interannual variations. Slopes (seasonal: 1.76 W m^{-2} K^{-1}, interannual: 2.09 W m^{-2} K^{-1}) are smaller than those from ERBE observations. In addition, slope uncertainties are smaller for CERES compared to ERBE for both cases. This can be explained by relatively smaller variances of residuals for CERES cases (in particular, seasonal variation case). These differences appear to imply that the rate of clear-sky longwave radiative damping varies depending on time period and/or dataset since inconsistent calibration methods and possible sensor degradation with time can affect the accuracy of computed radiative damping rates. It is also noted that the satellite infrared sensors only sample clear-sky scenes to avoid cloud contamination, producing higher value of OLR compared to climate models in cloudy convective regions [e.g., *Allan and Ringer*, 2003; *Sohn and Bennartz*, 2008]. As a result, the sampling difference between satellites and climate models may lead to a discrepancy in the computed slope. However, given the fact that those convective areas account for small fraction of the entire globe, the discrepancy appears to be small on a global scale. In addition, the use of different dataset for surface temperature may induce discrepancies in slope and uncertainty.

4. Summary

[25] In spite of significant biases in tropospheric temperature and humidity in climate models [*John and Soden*, 2007] and resultant compensating effects in simulating the clear-sky OLR, our analysis finds broad consistency between the observed and modeled rates of clear-sky OLR radiative damping. This consistency is noted over a broad range of observable sources of climate variations, suggesting that the strong correlations between water vapor and temperature necessary to generate such sensitivities are a robust feature of both models and observations. This analysis offers further evidence to support the ability of climate models to depict the physical processes related to the combined water vapor and temperature climate feedback.

[26] **Acknowledgments.** The authors would like to thank two anonymous reviewers for their constructive and valuable comments which led to an improved version of the manuscript. This research was supported by grants from the NOAA Climate Program Office and the NASA Energy and Water Cycle Program.

References

Allan, R. P. (2006), Variability in clear-sky longwave radiative cooling of the atmosphere, *J. Geophys. Res.*, *111*, D22105, doi:10.1029/2006JD007304.

Allan, R. P. (2009), Examination of relationships between clear-sky longwave radiation and aspects of the atmospheric hydrological cycle in climate models, reanalyses, and observations, *J. Clim.*, *22*, 3127–3145, doi:10.1175/2008JCLI2616.1.

Allan, R. P., and M. A. Ringer (2003), Inconsistencies between satellite estimates of longwave cloud forcing and dynamical fields from reanalyses, *Geophys. Res. Lett.*, *30*(9), 1491, doi:10.1029/2003GL017019.

Barkstrom, B., et al. (1989), Earth Radiation Budget Experiment (ERBE) archival and April 1985 results, *Bull. Am. Meteorol. Soc.*, *70*, 1254–1262, doi:10.1175/1520-0477(1989)070<1254:ERBEAA>2.0.CO;2.

Cess, R. D., et al. (1990), Intercomparison and interpretation of climate feedback processes in 19 atmospheric general circulation models, *J. Geophys. Res.*, *95*, 16,601–16,615, doi:10.1029/JD095iD10p16601.

Colman, R. (2003), A comparison of climate feedbacks in general circulation models, *Clim. Dyn.*, *20*, 865–873, doi:10.1007/s00382-003-0310-z.

John, V. O., and B. J. Soden (2007), Temperature and humidity biases in global climate models and their impact on climate feedbacks, *Geophys. Res. Lett.*, *34*, L18704, doi:10.1029/2007GL030429.

Kalnay, E., et al. (1996), The NCEP/NCAR 40-year reanalysis project, *Bull. Am. Meteorol. Soc.*, *77*, 437–471, doi:10.1175/1520-0477(1996)077<0437:TNYRP>2.0.CO;2.

Lindzen, R. S., and Y.-S. Choi (2009), On the determination of climate feedbacks from ERBE data, *Geophys. Res. Lett.*, *36*, L16705, doi:10.1029/2009GL039628.

Potter, G. L., and R. D. Cess (2004), Testing the impact of clouds on the radiation budgets of 19 atmospheric general circulation models, *J. Geophys. Res.*, *109*, D02106, doi:10.1029/2003JD004018.

Raval, A., and V. Ramanathan (1989), Observational determination of the greenhouse effect, *Nature*, *342*, 758–761, doi:10.1038/342758a0.

Slingo, A., J. A. Pamment, R. P. Allan, and P. S. Wilson (2000), Water vapor feedbacks in the ECMWF reanalyses and Hadley Centre climate model, *J. Clim.*, *13*, 3080–3098, doi:10.1175/1520-0442(2000)013<3080:WVFITE>2.0.CO;2.

Soden, B. J., and I. M. Held (2006), An assessment of climate feedbacks in coupled ocean-atmosphere models, *J. Clim.*, *19*, 3354–3360, doi:10.1175/JCLI3799.1.

Soden, B. J., I. M. Held, R. Colman, K. M. Shell, J. T. Kiehl, and C. A. Shields (2008), Quantifying climate feedbacks using radiative kernels, *J. Clim.*, *21*, 3504–3520, doi:10.1175/2007JCLI2110.1.

Sohn, B.-J., and R. Bennartz (2008), Contribution of water vapor to observational estimates of longwave cloud radiative forcing, *J. Geophys. Res.*, *113*, D20107, doi:10.1029/2008JD010053.

Uppala, S. M., et al. (2005), The ERA-40 re-analysis, *Q. J. R. Meteorol. Soc.*, *131*, 2961–3012, doi:10.1256/qj.04.176.

Weatherhead, E. C., et al. (1998), Factors affecting the detection of trends: Statistical considerations and applications to environmental data, *J. Geophys. Res.*, *103*, 17,149–17,161, doi:10.1029/98JD00995.

Wong, T., D. F. Young, M. Haeffelin, and S. Weckmann (2000), Validation of the CERES/TRMM ERBE-like monthly mean clear-sky longwave dataset and the effects of the 1998 ENSO event, *J. Clim.*, *13*, 4256–4267, doi:10.1175/1520-0442(2000)013<4256:VOTCTE>2.0.CO;2.

Zhang, M. H., J. J. Hack, J. T. Kiehl, and R. D. Cess (1994), Diagnostic study of climate feedback processes in atmospheric circulation models, *J. Geophys. Res.*, *99*, 5525–5537, doi:10.1029/93JD03523.

E.-S. Chung, B. J. Soden, and D. Yeomans, Rosenstiel School of Marine and Atmospheric Science, University of Miami, 4600 Rickenbacker Cswy., Miami, FL 33149, USA. (bsoden@rsmas.miami.edu)